Modeling and Development of the RF-Controlled Hollow Cathode Concept

Matthew L. Plasek,* Christopher J. Wordingham,* and Edgar Y. Choueiri†

Electric Propulsion and Plasma Dynamics Laboratory

Princeton University, Princeton, NJ 08544 USA

A promising new hollow cathode concept for high-power, long-lifetime electric thruster applications is explored using finite-element analysis to inform an experiment presently being constructed. This RF-Controlled Hollow Cathode concept adds radio-frequency power to a large-diameter cathode. To explore the concept's feasibility and behavior, numerical simulations were performed with a simplified two-dimensional model which captures the plasma, the thermionic emission, and the added RF power. It was found that by increasing the RF power, the centerline plasma density profile increased and its peak shifted upstream, resulting in enhanced thermionic emission from a greater emitter area, and thus supporting the promise of the concept for high-power, long-lifetime applications. It was also observed that a pronounced "jump" occurs in the plasma density and other parameters at a critical RF power, and its occurrence is strongly dependent on gas pressure. This beneficial jump behavior was attributed to a cavity resonance effect caused by the RF waves constructively interfering to sharply increase the electric field amplitude at a critical RF electric field phase and RF-reflecting plasma density depth.

Nomenclature

A_0	Theoretical Richardson-Dushman coefficient
D_0	Experimentally modified value of A_0
c_0	Speed of light in vacuum
$\bar{c}_\mathrm{e}$	Electron thermal velocity
e	Electron charge
n_e	Electron number density
n_i	Ion number density
E	Electric field
f_co	Waveguide cutoff frequency
f	Frequency of the RF source
J_te	Thermionic emission current density
J_i	Ion current density
J_e	Electron current density
J_r	Random electron current density
Γ	Emission to primary electron ratio
ρ_e	LaB_6 electrical resistance
$\dot{q}'''$	Joule heating of emitter material
q''_i	Heat flux due to ion current
q''_e	Heat flux due to electron current
q''_ex	Heat flux due to wall de-excitation
q''_w	Total emitter wall heat flux
k_B	Boltzmann's constant
k_0	Wave number

*Graduate Research Assistant, EPPDyL; Mechanical and Aerospace Engineering Dept., Student Member AIAA.

†Chief Scientist, EPPDyL; Professor, Applied Physics Group, Mechanical and Aerospace Engineering Dept.; Fellow AIAA.

a	Cathode radius
X'_{11}	Cutoff frequency constant
κ	Space charge-limited emission constant
T_{w}	Thermionic insert temperature
T_{e}	Plasma electron temperature
ϵ_0	Vacuum permittivity
ϵ	Relative permittivity
μ_0	Vacuum permeability
μ	Relative permeability
ϕ_{wf}	Material work function
$\Delta\phi_{\mathrm{SH}}$	Modification of work function due to Shottky Effect
ϕ	Plasma potential
ϕ_s	Plasma sheath potential
m_e	Electron mass
M_i	Ion/Neutral mass
x	Axial position
m	Mass
$\dot{m}$	Mass flow rate

Subscripts

i	Ion
e	Electron
te	Thermionic electron
ex	Excited
c	Critical

I. Introduction

State-of-the-art hollow cathodes meet the operational lifetime requirements of many solar electric propulsion and commercial satellite missions. These lifetimes have been demonstrated through extended life tests of up to 42,000 hours (42 kh) of operation.[1] However, NASA-proposed[2] nuclear electric propulsion missions to interplanetary destinations would require lifetimes approaching 100 kh. In addition to significantly extended lifetimes, power levels available for propulsion are expected to increase by an order of magnitude.[3] The U.S. Air Force Research Laboratory (AFRL) projects that electric thrusters will need to be capable of processing 100-200 kW of input power in the next few decades, dwarfing the 0.5 to 12 kW range of recent focus.[4] At the moderate specific impulse of AFRL interest (between 2000-6000 seconds), this translates to roughly 330-660 A of discharge current, which amounts to 1-2 orders of magnitude higher than currents commonly used in electric thrusters today (e.g. a nominal 20 A for a 6 kW laboratory Hall thruster).[5] The anticipation of higher power levels has led to the development of a 50 kW-class Hall thruster by NASA.[6] This Hall thruster has been recently tested up to 100 A of discharge current, stressing the need for higher performance cathodes explicitly designed to handle high discharge currents while providing extended operational life.

Goebel and Chu[7] experimentally showed that lanthanum hexaboride (LaB_6), bulk-emitting hollow cathodes can successfully achieve up to 300 A of discharge current with an expected life of 10-20 kh. Van Noord, et al.[8] describe the design and testing of a dispenser hollow cathode at 50 A with a predicted life of 100 kh. Even noting these selected advances, our stated requirements of 100 kh of operational lifetime and discharge currents approaching 700 A warrant the pursuit of novel cathode concepts that could potentially meet these goals in the mid-term.

In hollow cathodes, a sharp peak in the plasma density's axial profile along the centerline of the cathode corresponds to a small current attachment area (or area of dense plasma contact with the emitter).[9,10] This restriction in current attachment area results in high current densities and high temperatures within a limited axial depth inside the cathode, typically near the orifice downstream as shown schematically in Figure 1. As the plasma density drops off further upstream, the plasma is not dense enough to support the thermionic emission and thus the remainder of the upstream emission is space charge limited.[5] Ideally, the entire axial length of the emitter would be in contact with a dense plasma and would therefore be thermally-limited,

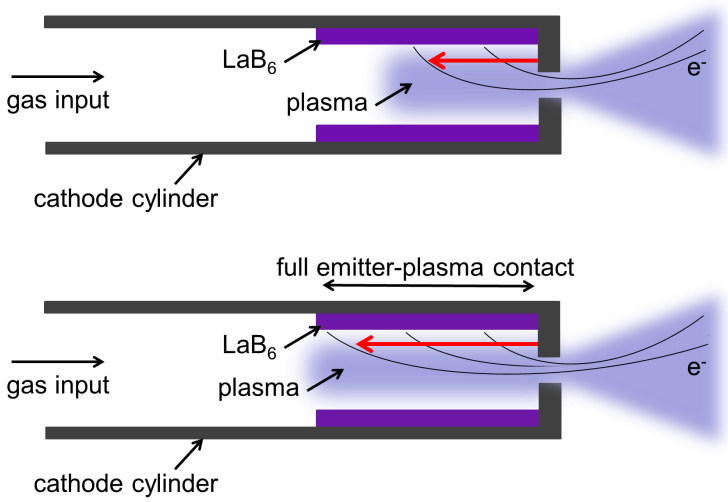

Figure 1. Schematic showing the side views of a basic cathode with limited current attachment area, or reduced plasma-emitter contact area, along the length of the emitter (top) compared to current attachment to the full emitter area (bottom). Dense plasma contacting the entire emitter area (bottom) allows for cathode operation completely in the desired thermally-limited emission regime. Gas flow is from left (upstream) to right (downstream) in all cathode figures.

or limited by the maximum temperature of the emitter, instead of being space charge limited. Completely thermally-limited emission requires that the plasma density and emitter temperature profiles be flatter and more uniform along the emitter length.

The life of a hollow cathode can be estimated to first order based on the evaporation rate of the emitter material which varies with the current density.[11,12] Therefore, by maintaining the same discharge current while increasing the current attachment area we expect the resulting lower peak emitter temperature to correspond to an increase in the lifetime of the cathode.[5] Meeting this goal allows the operator to choose some optimal balance between increasing the operational lifetime and increasing the discharge current to desired levels.

We are developing a proof-of-concept experiment for the RF-Controlled Hollow Cathode (RF-CHC) concept. Our findings here will be used to elucidate the concept and to guide the experiment presently being constructed. Our modeling results will be compared with future experimental data to verify our findings.

Our previous modeling[13] examined the concept of controlling current attachment along the length of the cathode's major axis by adding radio frequency (RF) energy to a hollow cathode's internal plasma. Our novel concept of the RF-Controlled Hollow Cathode relies on generating a dense plasma upstream that is comparable in density to the typical cathode plasma near the orifice. From our modeling[13] of a direct coaxial-cathode mating configuration of the RF-CHC, it was found that this configuration can lead to high percentages (>96%) of localized microwave power absorption when the RF inner coaxial conductor was positioned at an appropriate axial distance from the orifice based on the centerline plasma density profile. In the configuration analyzed, the RF inner coaxial conductor extending into the hollow cathode acted as a stinger, as approximately 62% of the RF power was absorbed within 2 mm of the inner coaxial conductor tip.

As our previous work[13] did not simulate RF power incident on a cathode plasma self-consistently, we could only describe the absorption of the RF power, not the self-consistent effect of the added RF power on the plasma and thermionic emission. We take these aspects into account here as we explore the feasibility and behavior of another configuration of the RF-CHC where a waveguide is mated directly to the upstream end of the cathode. We also address the previous assumption that the largest thermionic emission enhancement occurs where the RF power absorption is the greatest.

We start in Section II with a discussion of selected design considerations relevant to our simulations. Next, we present our numerical modeling methodology of the RF-CHC in Section III. We detail our results and discuss the physical insight captured from our simplified model in Section IV before summarizing our

findings.

II. Selected Design Considerations

The goal of the RF-Controlled Hollow Cathode is to expand the axial extent of the current attachment such that the emitter area operating in a thermally-limited regime is maximized, and, consequently, space charge-limited emission is minimized. In high current density hollow cathodes, space charge-limiting prevents the full utilization of the emitter which directly limits the cathode operational lifetime and the maximum discharge current.[10]

A minimum plasma density is needed to support a given electron emission current density. The maximum electron current density that a plasma can accept due to space charge-limiting effects at the emitter wall[10] is given by

$$J_e = \frac{\kappa}{2} n_i e \sqrt{\frac{k_B T_e}{m_e}} \approx \frac{1}{4} n_e e \sqrt{\frac{k T_e}{m_e}}. \tag{1}$$

Equation 1 tells us that space charge-limiting effects require that plasma densities greater than 10^{18} m^{-3} must exist in the cathode in order to reach an appreciable current density of around 2 A/cm^2 at the emitter as shown in Figure 2. Plasma densities on the order of 10^{19} m^{-3} are required to reach more substantial current densities that are no longer space charge limited and instead have transitioned into the thermally-limited regime. However, upstream plasma densities on the order of 10^{18} m^{-3} will still result in increased emission compared to a typical cathode configuration with insignificant upstream plasma densities (e.g., the NSTAR cathode[1]). For a lanthanum hexaboride (LaB_6), bulk-emitting hollow cathode, thermally-limited current densities are typically greater than 20 A/cm^2 corresponding to an emitter temperature of about 1700°C.[10]

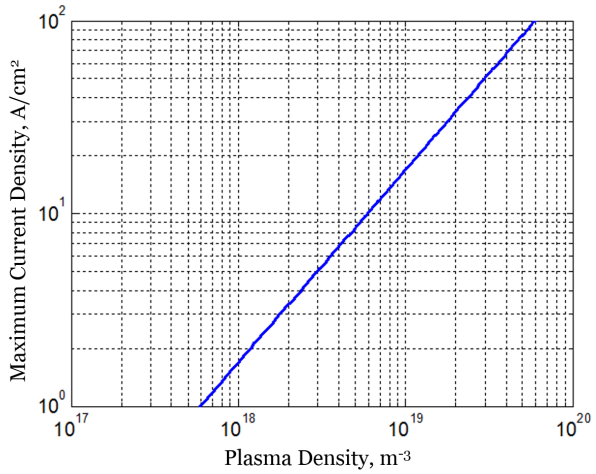

Figure 2. Maximum electron current density at the emitter wall as a function of plasma density. Argon gas and an electron temperature of 1 eV are assumed.

1. Adding RF Power to a Hollow Cathode

Achieving the necessary plasma densities in an upstream, RF-generated plasma depends on the frequency of the RF source. Typically, the maximum plasma density generated is related to the incident RF excitation frequency; at a critical plasma density, the corresponding plasma frequency is equal to the excitation frequency and the RF waves begin to be reflected. Due to this reflection, the maximum plasma density generated generally does not greatly exceed the incident excitation frequency.[14]

The RF frequency is also a major driver of the cathode design, and trade-offs between higher- and lower-frequency sources include waveguide size, source cost, and source availability. The RF-CHC configuration

we analyze in this paper mates a waveguide to the upstream end of the cathode, effectively treating the cathode tube as a cavity or a continuation of the waveguide. This is also the configuration of the cathode we are presently building for the experimental part of our study of this concept. Since the cathode is treated as a waveguide in this configuration, the cathode diameter is determined by the waveguide cutoff frequencies, which describe the ability of the RF waves to propagate inside the waveguide without being reflected or converted into modes outside the dominant transverse electric (TE_{11}) mode. The lower cutoff frequency for a TE_{11} mode in a circular waveguide[15] is given by

$$f_{\mathrm{co}} = \frac{X'_{11}}{2\pi a\sqrt{\mu\epsilon}}, \tag{2}$$

where $X'_{11} = 1.841$ and a is the cathode inner radius in meters. From Equation 2 we see that a larger cathode radius a gives a lower cutoff frequency f_{co}. Applied to reasonable cathode diameters, the waveguide cutoff frequencies constrain the source frequency to the microwave portion of the RF spectrum.

Cost, mass, and availability of microwave sources differ widely, both for lab experimentation and for use in a space environment. Higher frequencies at the output powers of interest generally correlate with higher system costs and lower availability. We selected an RF frequency of 8 GHz as a compromise between the cathode (waveguide) diameter, the RF source cost, and the effect on plasma density. As seen in Figure 3, a source frequency of 8 GHz corresponds to a critical plasma density of about 8×10^{17} m^{-3}, near our minimum goal of the 10^{18} m^{-3}.

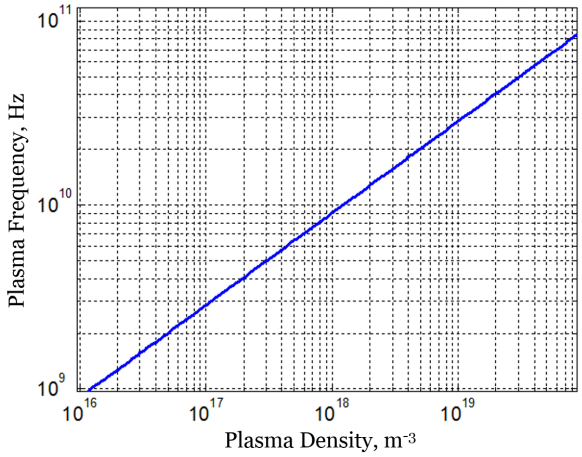

Figure 3. Electron plasma frequency corresponding to plasma density. A plasma density of about 8×10^{17} m^{-3} will reflect incident microwaves of 8 GHz.

The input power also presents a compromise between minimizing the spacecraft power required to operate the additional RF subsystem and applying adequate RF power to achieve the desired result. Our incident RF power range of interest is ten to several hundred watts while the discharge power from thermionic emission is in the hundreds to thousands of watts assuming a discharge voltage of around 20 volts. Clearly, the added RF power is marginal relative to the power output from the thermionic emission current. The major contribution expected from the added RF power is to change the upstream cathode conditions in such a way that the overall thermionic emission is increased. The main processes by which this can occur are (1) increasing the plasma density in the upstream cathode to prevent space charge limitation and (2) increasing the upstream cathode emitter temperature via higher ion and electron bombardment rates.

To efficiently transfer RF source power to the emitter region the waveguide can be impedance matched to the cathode plasma load with common tuning mechanisms (e.g. a triple stub tuner).[16,17] Figures 4 and 5 show side cutaway views of an accurately-proportioned RF-CHC waveguide configuration. Depicted by the orange arrow in Figure 5, microwaves travel into the cathode tube and through a thin disc made of hexagonal boron nitride (white in color). The disc serves both as a low-loss microwave window and a gas barrier in

the cathode waveguide. Neutral gas is injected through the gray stainless steel base into an annular region between the two black graphite cylinders, where it travels downstream and then moves radially inward into the cathode tube immediately after the microwave window. The two-dimensional version of this path is depicted by the light blue arrows in Figure 5. The emitter region, where the thermionic emission plasma is generated, is shown as purple LaB_6 in Figure 4 and as an example two-dimensional plot of the simulated plasma density in Figure 5.

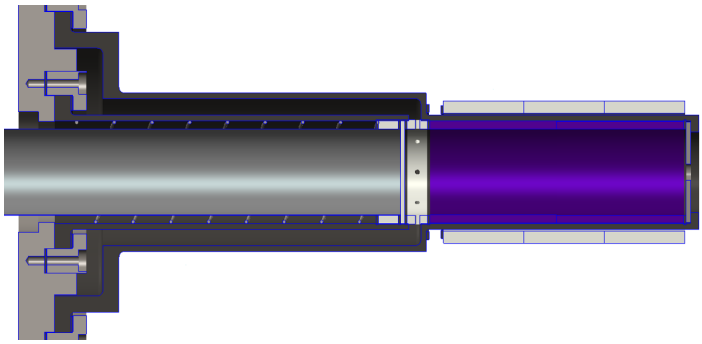

Figure 4. Side cutaway view of the RF-CHC waveguide configuration.

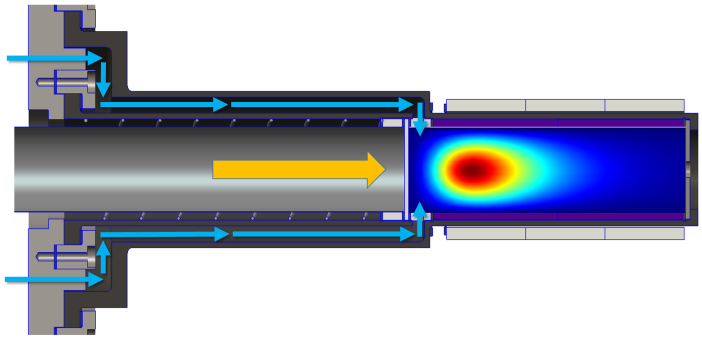

Figure 5. Side cutaway view of the RF-CHC waveguide configuration. Orange arrow depicts microwave propagation, light blue arrows depict neutral gas injection path, and the downstream emitter region on the right shows an example plasma density simulation result, matching the bounds of our cathode cavity model.

As mentioned in our previous paper,[13] with the addition of a microwave source comes the addition of a source cathode which could become a life limitation. However, currently available space-qualified microwave sources (e.g. traveling wave tubes) have lifetimes which extend well beyond the stated cathode lifetime goal of 100 kh.[18,19] Microwave source thermionic cathodes with lifetimes >100 kh are usually mixed metal matrix cathodes and can achieve such lifetimes due to relatively low operating temperatures (<1000°C) and low current densities (1-2 A/cm^2).[18]

2. Cathode Size

Besides the addition of RF power, another unique feature of the RF-CHC waveguide configuration is its inner diameter of 2.7 cm, which is approximately twice as large as any other cathode developed to date. The next largest hollow cathode we are aware of is Goebel and Chu's LaB_6 hollow cathode[5,12] with an insert inner diameter of 1.27 cm. For comparison, Goebel and Chu's[5] cathode can theoretically obtain approximately 400 A of discharge current from 20 cm^2 of emitter area assuming a uniform emitter current density of 20 A/cm^2, while at the same uniform current density the RF-CHC could achieve approximately 1360 A from its 68 cm^2 of emitter area.

The large diameter of the RF-CHC is driven by the need for the diameter to contain the circular waveguide cutoff wavelength for an 8 GHz RF frequency including a margin. In addition to analyzing the feasibility and behavior of the added RF power to a hollow cathode, we can also analyze the behavior of a significantly larger hollow cathode than those tested to date. A larger-diameter cathode is directly relevant to our stated goals and is a strategy suggested by many authors.[8,20–22] By using a larger diameter, and therefore a larger emitter area, we can achieve higher maximum discharge currents and lower current densities. As noted in Ref. 23, lower current densities tend to reduce high-energy ion production and "plume mode" oscillations. Plasma oscillations and the production of energetic ions that have been linked with so-called plume mode operation can critically erode the cathode keeper and cathode, causing off-design operation and eventual failure.[23–27]

Other effects of a larger-diameter hollow cathode include lower operating pressures, less sensitivity to changes in neutral gas flow rate, and the need for higher flow rates to reach modest pressures. For example, using a one-dimensional Poiseuille flow model[10] the RF-CHC is found to reach approximately 2 Torr along most of the axial emitter length from 70 sccm of argon input assuming an orifice diameter that is 25% of the cathode inner diameter. In 2010, Goebel and Watkins[22] found that as the internal neutral gas pressure is reduced, the upstream depth of current attachment increases and the axial plasma density profile along the emitter length is flattened.

Another predicted effect is that a larger cathode will operate at lower temperatures[20] due to a shift in the power balance due to charged particle bombardment and microwave power deposition balanced with losses from thermionic cooling, thermal conduction along the cathode tube, and radiation from the surface. Lower emitter temperatures and decreased axial temperature gradients benefit the expected lifetime of the cathode. Assuming plume mode can be avoided by using the appropriate orifice diameter, mass flow, and external injection of neutral gas into the plume,[7,28] both a larger cathode diameter and added RF power are expected to increase the maximum discharge current while lowering current densities.

3. Lanthanum Hexaboride Bulk-Emitting Cathodes

LaB_6 is a bulk emitter and needs neither a supporting matrix nor any chemical reactions to maintain its low work function unlike dispenser-type cathodes. LaB_6 has been used as a bulk emitter in Russian cathodes for decades and more recently in the U.S. due in part to the emitter's better resistance to poisoning compared to dispenser cathodes.[10] LaB_6's higher work function[29] (about 2.67 eV) requires higher temperatures to reach the same current density as dispenser cathodes. However, simulations[12,21] using lifetime models have shown that LaB_6 actually achieves a longer life. This longer life is due to a lower evaporation rate below about 15 A/cm^2 and because more emitting material is available for the same insert size relative to dispenser cathodes. For comparison, tungsten has an order of magnitude higher evaporation rate[21] than both dispenser and bulk emitter cathodes up to current densities of 30 A/cm^2. There is also some indication that LaB_6 cathodes could exhibit recycling of the bulk emitter material similar to the barium recycling seen in dispenser cathodes that benefits the cathode's operational lifetime.[30]

Due to higher poisoning resistance than dispenser cathodes, longer simulated life, and demonstrated ability to reach high current densities above 20 A/cm^2 and high discharge currents of up to 300 A,[5] we have chosen LaB_6 as the emitter for our cathode concept and experimentation.

III. Numerical Modeling

A. Schematic Representation

The computational model we developed relies on a simplified version of the RF-CHC concept, shown in Figure 6 below. The model used is two dimensional rather than axisymmetric because of a known issue present in the microwave plasma model of COMSOL at the time of this writing.

B. Computational Grid

A structured quadrilateral mesh with approximately 7000 domain elements (COMSOL uses the finite element method) was used for all simulations and is shown in Figure 7; after performing a grid sensitivity study by refining the grid by a factor of two in each node distribution, we determined that the grid shown offered

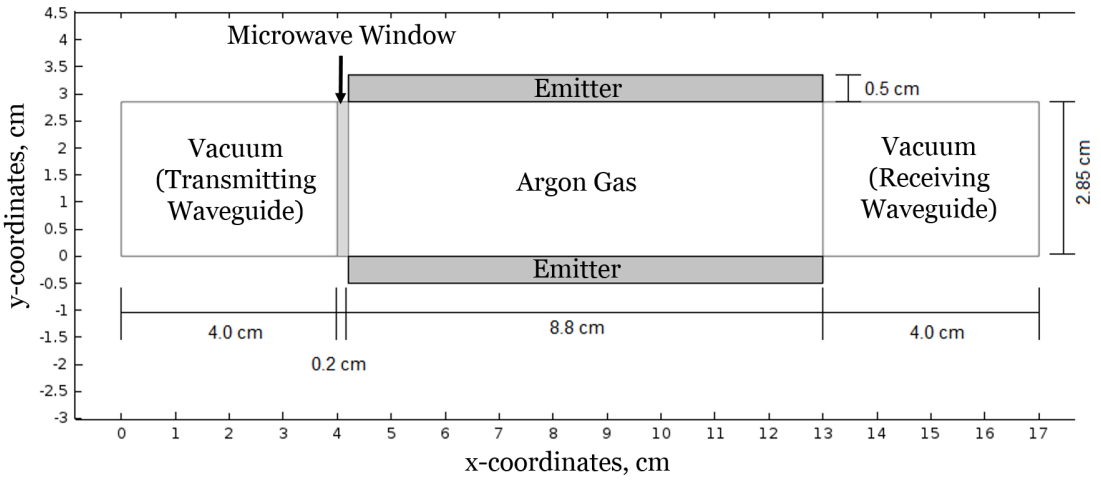

Figure 6. RF-CHC Schematic Representation

the best balance of computation time and simulation accuracy. Simulation variables of interest, e.g. plasma density, varied by less than 2% when the grid density was increased.

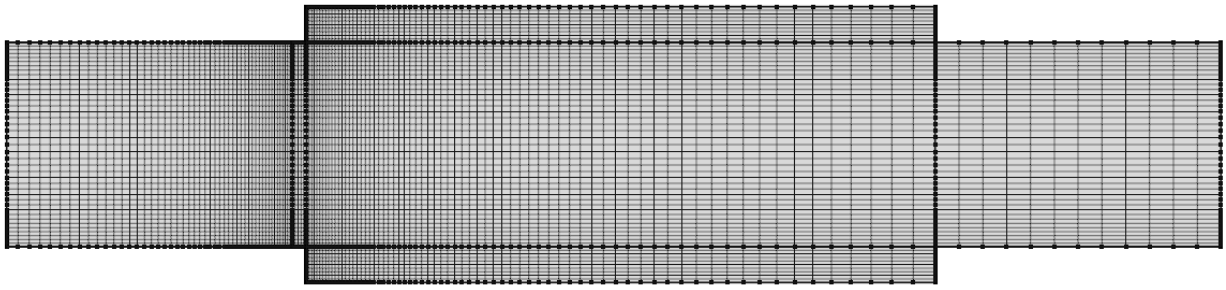

Figure 7. RF-CHC Computational Grid, refined near regions of expected sharp transition, such as the plasma-surface boundaries and the microwave window.

C. Computational Model

The use of commercial software encapsulates functionality, reducing the time and effort required to create a working model, but also reduces the degree of customization available to the user. As such, the boundary conditions chosen are modified versions of those given in previous computational cathode studies.[10,31]

1. Flow and Neutral Pressure

In the computational model, argon gas is assumed to enter via the microwave window, which was found to be a good approximation because the simulation results were insensitive to the velocity field within the cathode (likely due to orifice exclusion). Having made this observation, we do not solve for the fluid velocity field. Instead, we model the effect of increasing argon mass flow by the dominant pressure determined using

a Poiseuille flow model[10,32] for an orifice diameter that is 25% of the cathode emitter inner diameter. The orifice itself is not contained in the model, and the plasma region modeled ignores effects due to the presence of an orifice, excluding its effect on the average neutral pressure.

2. Heat Transfer

Heat transfer within the cathode walls is solved for a stationary solution at each time step of the transient microwave plasma simulation (the heavy species temperature is assumed constant throughout the plasma). This solution method significantly reduces the total simulation time required for a steady-state solution. The outer boundaries of the emitter material are treated as radiative surfaces, approximating poor thermal contact between the emitter and the cathode tube, and thermal conduction is restricted to within the emitter material. The inner boundaries of the emitter are in contact with the cathode plasma, and the heat flux into the emitter is determined using the plasma simulation detailed in Section 4. The combined heating and cooling due to the plasma fluxes and thermionic emission at the emitter wall is given by

$$q''_{\text{wall}} = q''_{\text{i}} + q''_{\text{e}} + q''_{\text{ex}} - q''_{\text{te}}, \tag{3}$$

where the heat flux due to de-excitation at the wall, q''_{ex}, was found to be negligible, and is excluded from further calculation. In addition to the plasma heat flux into the emitter, heating due to electrical conduction of the emitted current is modeled using a volumetric heat source,

$$\dot{q}''' = J_{\text{te}}^2 \rho_{\text{e}}, \tag{4}$$

where the electrical conductivity of LaB_6 is taken from a linear approximation of the temperature-dependent data given by Lafferty.[29] Finally, as shown in the schematic, the orifice region is ignored, but given the size of the RF-CHC (limited by the waveguide properties required for the target RF source), the most prominent means of insert heating will likely not be orifice heating,[10] but rather electron and ion impacts with the emitter.

3. Microwave Propagation

In our model, an input rectangular waveguide excited at the TE_{01} mode provides RF power to the cathode via the microwave window. For a rectangular waveguide, the fundamental transverse electric (TE) mode is the TE_{01} mode, but had we used an axisymmetric model we would have used the corresponding fundamental mode for a circular waveguide, the TE_{11} mode. The inner cathode walls (including those of the emitter material) are considered to act as perfectly conducting surfaces for the purposes of microwave propagation, but this assumption should have little impact on the results as microwave reflection and absorption within the plasma/gas is likely the dominant means of attenuation. An exit waveguide is also included for the purposes of calculating microwave absorption in the cathode plasma.

4. Plasma Model and Wall Fluxes

Much of the plasma model, including the RF power absorption, is encapsulated in COMSOL's microwave plasma model. In addition to the wall boundary conditions for the thermal model mentioned earlier, the plasma-contacting walls are set to a constant electric potential. The primary modifications to COMSOL's built-in model are comprised by the plasma heat flux coupling to the wall. The driving mechanism behind hollow cathode current generation is thermionic emission. Richardson's original work on the subject and its re-visitation by several other authors[33] eventually resulted in the Richardson-Dushman equation:[10,33]

$$J_{\text{te}} = A_0 k_{\text{B}} T_{\text{w}}^2 exp\left(\frac{-e\phi_{\text{wf}}}{k_{\text{B}} T_{\text{w}}}\right), \tag{5}$$

where the universal constant $A_0 = 120.17 \frac{A}{cm^2 K^2}$ is typically replaced by an experimentally determined constant, $D_0 = 29 \frac{A}{cm^2 K^2}$, where the value shown is that found by Lafferty[29] for lanthanum hexaboride. Because the thermionic emission from the insert is driven by the temperature of the emitter, the wall heat fluxes due to the plasma are of critical importance to our model. The fluxes used in our analysis are modified

from previous modeling studies and expressed in the equations below. Equation 6 gives the heat flux to the emitter wall due to the ion flux,[10]

$$q_{\mathrm{i}}'' = J_{\mathrm{i}}\left(\epsilon_{\mathrm{i}} + \phi_{\mathrm{s}} + \frac{1}{2}\frac{k_{\mathrm{B}}T_{\mathrm{e}}}{e} - \phi_{\mathrm{wf}}\right), \tag{6}$$

which is comprised by the energy released during recombination (assumed to occur for all ions striking the wall), the thermal energy gained by the ions during their acceleration in the pre-sheath, the energy gained by the ions as they are accelerated through the sheath potential (whose approximation is discussed later), and the energy removed from the wall by the recombination electron. Ions are assumed to strike the wall at the Bohm velocity for the purposes of calculating the flux to the wall, and the number density is computed by COMSOL. The wall heating due to the electron flux is given by[10]

$$q_{\mathrm{e}}'' = (2T_{\mathrm{e}} + \phi_{\mathrm{wf}})\, J_{\mathrm{r}} exp\left(\frac{-\phi_{\mathrm{s}}}{T_{\mathrm{e}}}\right), \tag{7}$$

where J_{r} is the random thermal electron current density to the wall,[10]

$$J_{\mathrm{r}} = \frac{1}{4} e n_{\mathrm{e}} \bar{c}_{\mathrm{e}}, \tag{8}$$

and the electron density, n_{e} is evaluated in the plasma at the sheath edge. Since COMSOL already computes the electron density at the wall, this value is simply used instead and the exponential term that accounts for the sheath variation of the electron density in Equation 7 is dropped. Finally, the heat flux removed from the wall due to thermionic emission cooling is

$$q_{\mathrm{te}}'' = J_{\mathrm{te}}\left(\phi_{\mathrm{wf}} + 2\frac{k_{\mathrm{B}}T_{\mathrm{w}}}{e} - \phi_{\mathrm{s}}\right), \tag{9}$$

which accounts for the energy removed from the emitter due to the work function and the average thermal energy of the electrons that escape the wall, which is twice the wall temperature in eV.[33] Equation 9 also adds the heat produced by the emission electrons being accelerated through the sheath, as the sheath is too small to be captured by our computational grid in COMSOL.

5. Sheath Model

In order to evaluate the expressions in Section 4, we need an estimate of the sheath potential. Due to the cold electron emission at the wall, the sheath potential is reduced and possibly spatially non-monotonic. This is especially true in the limiting case of space charge-limited emission, which is likely to occur for the lower plasma densities in the range of consideration for the RF-CHC. Our model for the sheath potential is due to Hobbs,[34] and is formulated for a floating wall, but the same effect applies for a fixed-potential wall (the reduction of the sheath potential due to the cold emission electrons emanating from the emitter wall). If we assume that the ratio of emission to primary plasma electrons is low ($\Gamma << 1$), the sheath potential would be approximated by

$$\phi_{\mathrm{s}} = \frac{-k_{\mathrm{B}}T_{\mathrm{e}}}{e} ln\left[\frac{1-\Gamma}{\sqrt{2\pi m_{\mathrm{e}}/M_{\mathrm{i}}}}\right], \tag{10}$$

where Γ is the ratio of emission to primary electrons. This is highly unlikely to be the case at the thermionic temperatures considered, and we therefore make the opposite assumption. We assume that the wall emission is space charge limited, and that the ratio of emission to primary electrons takes on the following critical value,[34]

$$\Gamma_{\mathrm{c}} = 1 - 8.3\left(\frac{m_{\mathrm{e}}}{M_{\mathrm{i}}}\right)^{1/2}, \tag{11}$$

which is approximately 0.97 for argon. This emission-to-primary-electron ratio results in a sheath potential given simply in terms of the electron temperature (easily extracted from the COMSOL output):

$$\phi_{\mathrm{c}} = -1.02\frac{k_{\mathrm{B}}T_{\mathrm{e}}}{e}. \tag{12}$$

Using this approximation for the sheath potential, we can calculate the heat fluxes to the emitter wall for the RF-CHC. Given that the grid element size is too large to effectively capture the sheath, the average energy of the emitted electrons is set higher than that given by twice the wall temperature, as the sheath acceleration must also be considered. The value chosen for the thermionic electron energy was fixed at 3 V because a variable energy based on the sheath potential caused the simulation to become unstable. This effectively lumps the cold-electron sheath effects into the wall boundary itself. Finally, we note that the effect of the RF electric field on the sheath near the microwave window and the modification of the work function[35] due to the Schottky Effect, $\Delta\phi_{SH}$, are ignored.

IV. Results and Discussion

The first goal of our modeling is to gauge the feasibility of creating a substantial effect on the internal cathode plasma by adding RF power. The second goal is to gain insight into the trends that emerge from the modeled physics by comparing the results of different simulated cases. We are concerned primarily with the relationships between parameters and to a lesser extent with the accuracy, which we approach from an order-of-magnitude perspective as we are using a simplified model without an orifice or external plasma coupling.

The feasibility of the RF-CHC depends heavily on whether the added RF power can significantly affect the internal cathode plasma. From our modeling we found three major effects that result from the addition of RF power:

1. With increasing RF power the plasma density increases over most of the emitter length, favoring the axial locations at which the plasma density and emitter temperature peak,

2. Increasing the RF power causes the axial location of densest plasma region to shift upstream on the order of millimeters to centimeters, and

3. A "jump" occurs in the plasma density, upstream electron temperature, emitted current, and RF power absorption which is dependent on the neutral gas pressure, the phase of the incident electric field, and the incident RF power.

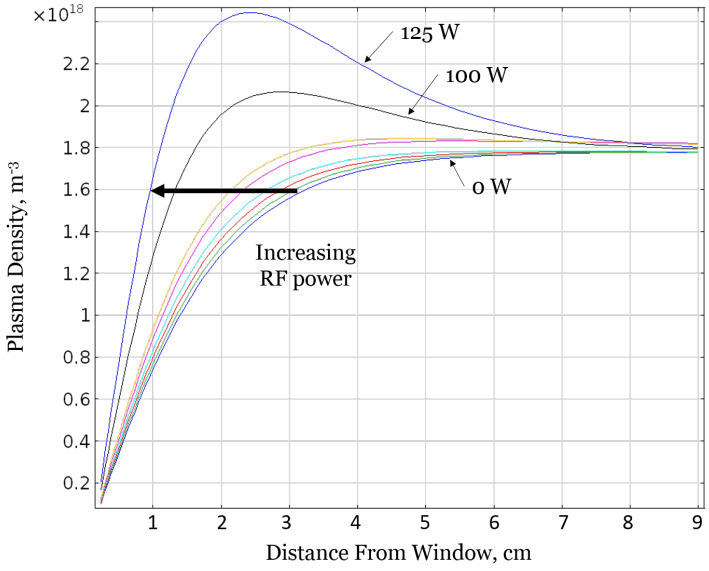

Figure 8. Plasma density profiles versus distance from the microwave window for a uniform pressure of 1.5 Torr (corresponding to an argon flow rate of 40 sccm). As the RF power increases, a significant plasma density extends further upstream (shown by the bold arrow). The upstream microwave window edge is on the left (Distance From Window = 0 cm), while the downstream orifice is on the right (Distance From Window = 9.0 cm).

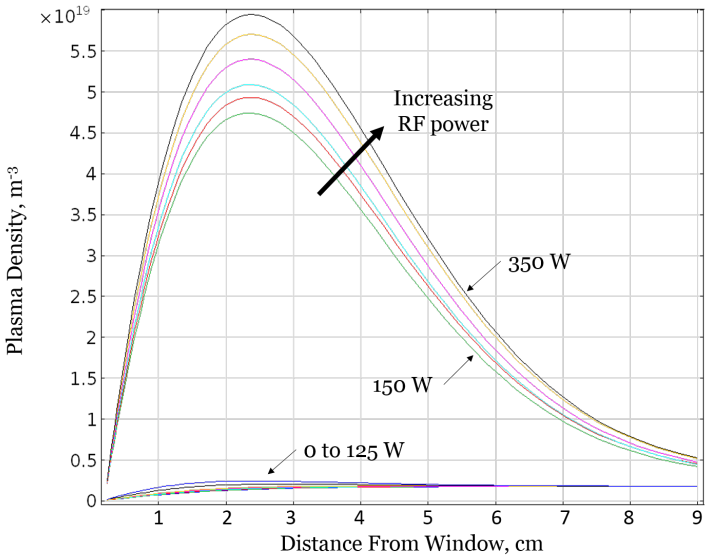

Figure 9. Plasma density profiles versus distance from the microwave window for a uniform pressure of 1.5 Torr (corresponding to an argon flow rate of 40 sccm). As the RF power increases further, plasma density increases preferentially at the axial depth of the maximum plasma density and peak emitter temperature. The upstream microwave window edge is on the left (Distance From Window = 0 cm), while the downstream orifice is on the right (Distance From Window = 9.0 cm).

Let us start by examining our first two findings of the increasing plasma density and of the plasma density profile shifting upstream with increasing RF power input. Figure 8 shows the centerline plasma density profile along the emitter length for a uniform pressure of 1.5 Torr (200 Pa) corresponding to an argon flow rate of 40 sccm (or 1.2 mg/s of argon). In Figure 8 we can see that the plasma density profile increases gradually for less than 100 W of RF power and shifts upstream with increasing RF power input. For example, at 3 cm from the microwave window with no RF power added the plasma density is 1.6×10^{18} m^{-3} and with 125 W of RF power input, the same plasma density shifts 2 cm upstream along the bold arrow to 1 cm from the window. Continuing the example, the original location at 3 cm increased in plasma density from 1.6×10^{18} m^{-3} at zero RF power to 2.2×10^{18} m^{-3} at 125 W RF power while the location 1 cm from the window increased from about 0.7×10^{18} m^{-3} at zero RF power to about 1.7×10^{18} m^{-3} at 125 W. However, in the downstream region between 8 and 9 cm from the microwave window we can see there is little change in the plasma density profile due to the addition of RF power.

Although Figure 8 shows a beneficial increase and upstream shift in the plasma density profile, the figure does not include the aforementioned drastic "jump" behavior. This "jump" in plasma density occurs at higher RF powers and is captured in Figure 9. We can see in Figure 9 that the plasma density preferentially increases about a peak at approximately 2.5 cm from the microwave window, corresponding to a peak in emitter temperature. The maximum plasma density increases by an order of magnitude to 4.7×10^{19} m^{-3} from an RF power increase from 125 to 150 W and the density continues to increase with RF power although only by about 30% over the next 200 W increase in RF input power. Even the region from 8 to 9 cm downstream of the window shows change, doubling in plasma density over the jump, although this is small compared to the maximum increase.

Figures 10 and 11 show similar plasma density profiles for a higher uniform pressure of 2.5 Torr (333 Pa), corresponding to an argon flow rate of 110 sccm (or 3.3 mg/s). Similar behavior results, but we note that the jump is dependent on pressure; at this higher pressure the jump occurs between 20 and 30 W of RF power, much lower than the 125 to 150 W for a pressure of 1.5 Torr. This tells us that increasing RF power can decrease the cathode flow rate required to cause a jump into a high-density operating regime. This high-density mode is beneficial as it significantly raises the space charge emission limit over most of the emitter area.

A two-dimensional representation of the same data from the 2.5 Torr cases without the jump can be seen in Figure 12 and a post-jump case at 2.5 Torr is seen in Figure 13. We note that the high-plasma-density region (for example, the region with plasma densities greater than 0.8×10^{19} m^{-3} colored in red)

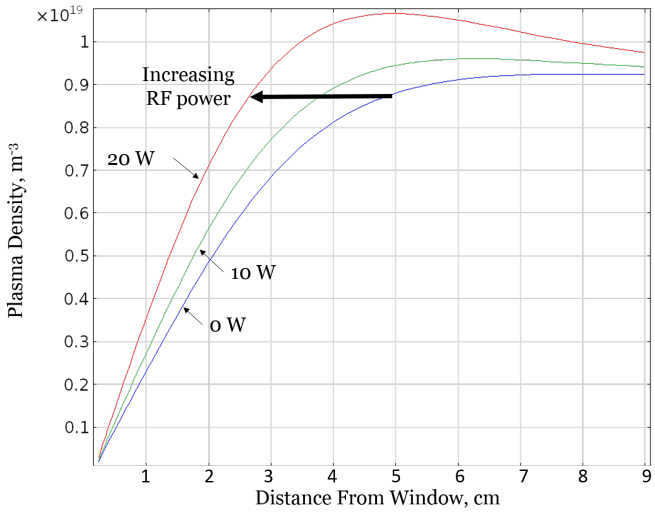

Figure 10. Plasma density profiles versus distance from the microwave window for a uniform pressure of 2.5 Torr (corresponding to an argon flow rate of 110 sccm). As the RF power increases, a significant density extends further upstream (shown by the bold arrow). The upstream microwave window edge is on the left (Distance From Window = 0 cm), while the downstream orifice is on the right (Distance From Window = 9.0 cm).

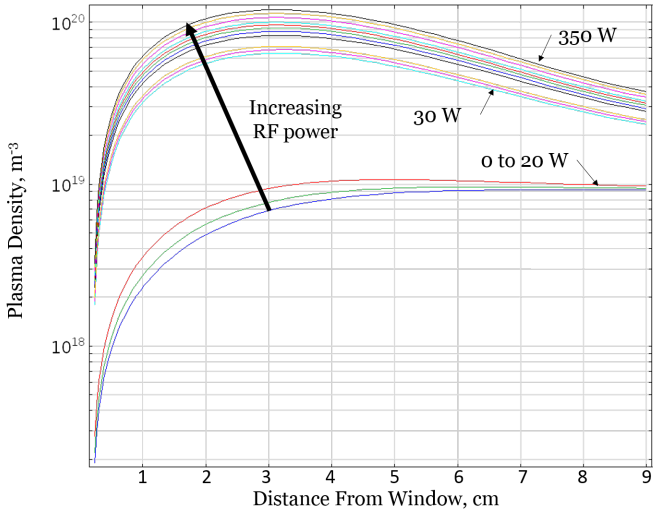

Figure 11. Plasma density profiles versus distance from the microwave window for a uniform pressure of 2.5 Torr (corresponding to an argon flow rate of 110 sccm). As the RF power increases further, plasma density increases preferentially near the depth of the maximum plasma density. The upstream microwave window edge is on the left (Distance From Window = 0 cm), while the downstream orifice is on the right (Distance From Window = 9.0 cm).

shifts markedly upstream with increasing RF power from Figure 12a at zero RF power to 12c at 20 W of RF power. The centerline average and maximum plasma densities visibly increase as well.

We observed that the RF power absorption takes place over 1 cm or less from the microwave window before the RF power is reflected by the overdense plasma, undergoes further absorption in the 1 cm region, and then the remainder of the RF power travels back upstream creating a standing wave interference pattern. This power absorption increases the electron temperature in the same region but affects the entire plasma and the cathode's total thermionic emission. Therefore we suggest that the assumption that the greatest enhancement of thermionic emission and plasma density will occur in the region where the majority of the RF power absorption takes place, or the location of the highest incident electric field, is not an accurate

assumption in a hollow cathode environment.

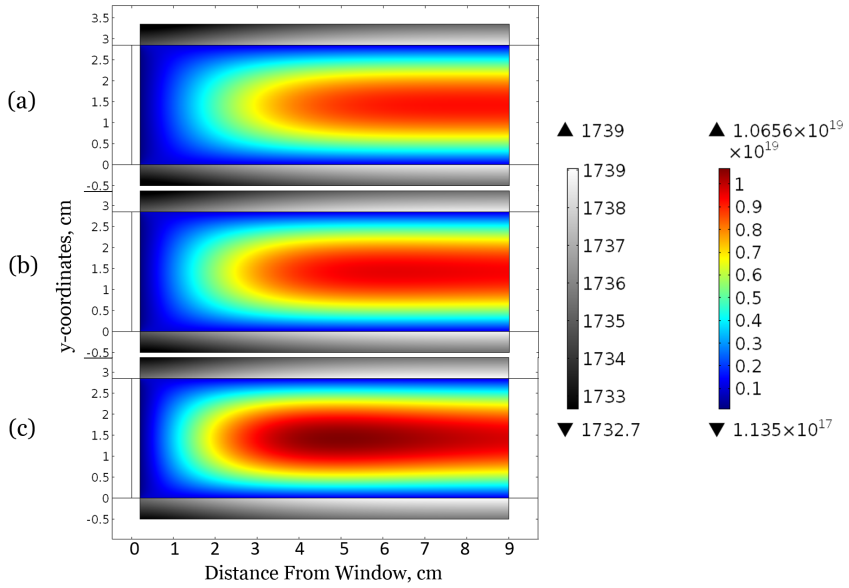

Figure 12. A two-dimensional representation of the plasma density profile versus distance from the microwave window corresponding to the curves in Figure 10. The three plots are using the same color scaling to compare increasing RF powers moving down with (a) 0 W, (b) 10 W, and (c) 20 W. Note that the centerline plasma density is increasing and the densest region moves upstream with increasing RF power. Surface plots of the emitter temperature are shown in grayscale above and below the plasma density surface plots.

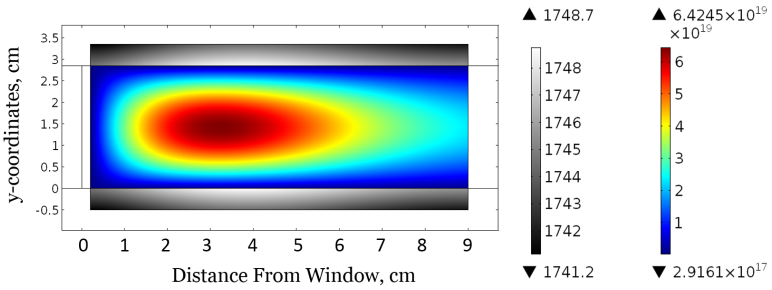

Figure 13. Continuing the increase in RF power from Figure 12, this two dimensional plot has an incident RF power of 30 W and has made a significant jump in plasma density. This figure has a different color scaling than the pre-jump plots in Figure 12. Surface plots of the emitter temperature are shown in grayscale above and below the plasma density plot.

We can qualitatively compare the zero RF power case in Figure 12a to other LaB_6 hollow cathodes[7] and find that the emitter temperature profile in our model also starts at a minimum temperature upstream and increases to the maximum value at the downstream end. Our modeling shows a slight temperature gradient in the LaB_6 emitter material at steady-state with the highest temperature corresponding to the location of the peak plasma density along the centerline. This behavior is expected due to greater thermionic emission rates from higher emitter temperatures as per Equation 5. Although effectively an estimation, the 1700 to 1800 K emitter temperatures from our modeling of the RF-CHC are lower than those in other LaB_6 cathodes. Goebel and Chu's[7] largest hollow cathode operates with an orifice (and assumed emitter) temperature greater than about 1800 K at its lowest measured discharge current (around 25 A). This temperature discrepancy is likely due to a combination of a simplified model that does not include orifice effects, the radiative thermal boundary conditions that can be varied substantially in our model and in an actual experiment, and the RF-CHC's large diameter, which we expect to result in comparatively lower operating temperatures.[20] We also expect the peak plasma density to penetrate a significant depth upstream due to the large diameter and

lower gas pressures present,[10] and this behavior is seen in Figure 12a. The lower operating temperatures and the significant upstream penetration of a dense plasma are beneficial in reducing the peak emitted current density at a given discharge current.

Figure 13 is a continuation of the increasing RF power at 2.5 Torr from Figure 12. Figure 13 shows an order-of-magnitude jump in the maximum plasma density (using a different color scale than Figure 12) and a significant upstream shift in the peak of the density profile at an RF power input of 30 W. The emitter temperature has increased only marginally but shows a new trend in the temperature gradient; the temperature no longer peaks at the downstream end but more centrally, corresponding to the peak plasma density. The higher plasma densities that occur after the jump, on the order of 10^{19} m^{-3} in Figure 13, meet our stated goal and allow current densities of 20 A/cm^2.

We note that there is a peak in the plasma density's axial profile in the high density operating regime with the maximum density at least double that of the downstream minimum. This peak may result in a premature depletion of the emitter material at the location of the maximum plasma density, similar to the barium depletion observed near the downstream end in dispenser cathodes.[30] Considering that the simulated plasma density peak is much less sharp than that of the typical dispenser cathode,[30] and that the current densities are much lower overall, we do not expect this to be a limiting factor in the lifetime of the RF-CHC. With no added RF power the plasma density profile does not exhibit this peak and is relatively flat until it drops off upstream. This uniformity is nearly ideal, but does not take into account orifice effects. However, it is a reasonable approximation of an upstream cathode section for a large-diameter cathode.

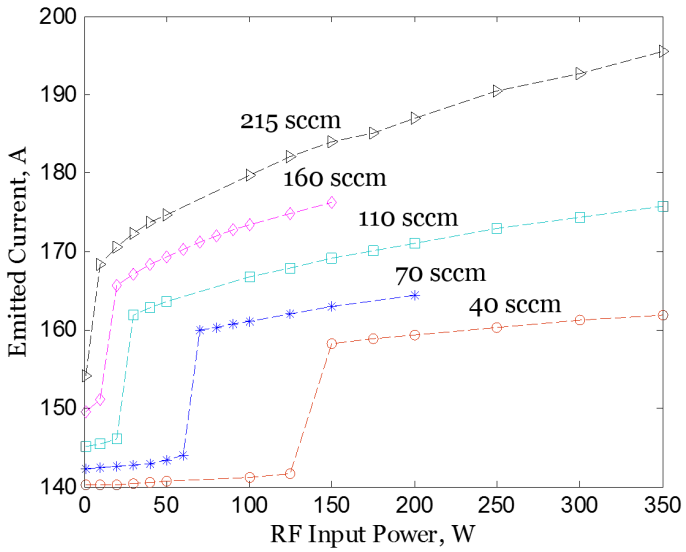

Figure 14. Emitted current versus RF power for five different flow rates corresponding to pressures used in our simulations. Note the clear jump in emitted current and the critical jump point's dependence on RF power and flow rate.

The "jump" is shown for a variety of argon flow rates in Figure 14, where we plot integrated current emitted from the walls as a function of RF power. The emitted currents are seemingly low, but the operating temperatures we observed are also notably low and correspond to the appropriate discharge currents. As noted above, the radiative thermal boundary conditions applied to the emitter may not correspond to experimental values and could offset the steady-state simulated temperature significantly.

The jump's dependence on the gas pressure (therefore on flow rate and orifice size) and on RF power can be seen in Figure 14. We explored the behavior of the critical jump point and found that the jump is distinctly sharp and occurs over less than 1 W of RF power increase. However, we do not believe the jump is due to numerical instabilities as the model's convergence near the jump is stable and predictable. Our model does not capture orifice effects or coupling to the external plasma, so we also do not expect the jump to be related to a plume-to-spot mode transition typically found in hollow cathodes.

Having observed the changes that the plasma undergoes during the jump transition, and a dependence of the critical jump RF power on waveguide length, we attribute the onset of the jump condition to an RF

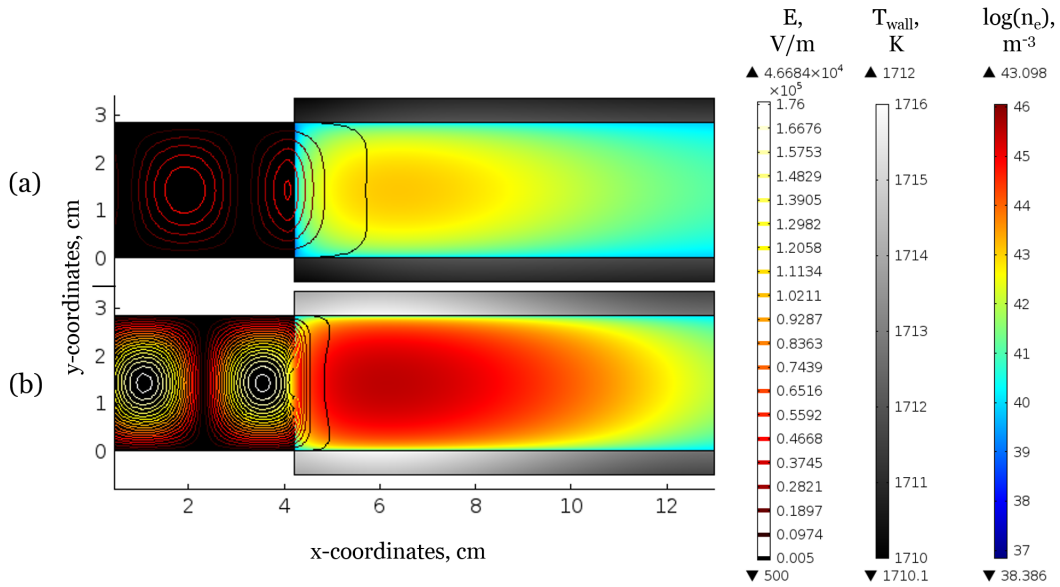

Figure 15. Two-dimensional plots pre-jump (a) and post-jump (b) of the emitter temperature (T_{wall}), the log of the plasma density, and overlayed contours of the RF electric field amplitude. The upstream waveguide is on the left (black background), with the emitter shown above and below the cathode cavity region, downstream of the waveguide-to-cathode-cavity transition. Note that the structure of the RF electric field amplitude changes and the amplitude increases significantly from before the jump (a) to after the jump (b). This corresponds to substantial changes in plasma density and emitter temperature.

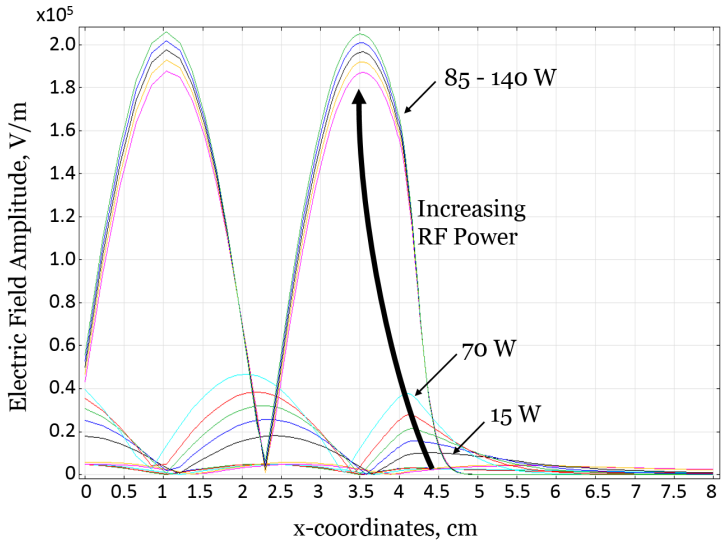

Figure 16. RF electric field amplitude curves for different RF powers as a function of waveguide position. At a critical RF power the electric field amplitude jumps in magnitude due to a cavity resonance condition. Note that the structure of the electric field amplitude changes significantly after the jump.

cavity resonance that occurs within the cathode. As described previously, we observe that increasing the RF power added to a hollow cathode shifts the maximum plasma density upstream. Hence, the critical plasma density at which the incident RF waves are reflected also shifts upstream. This axially-moving critical plasma

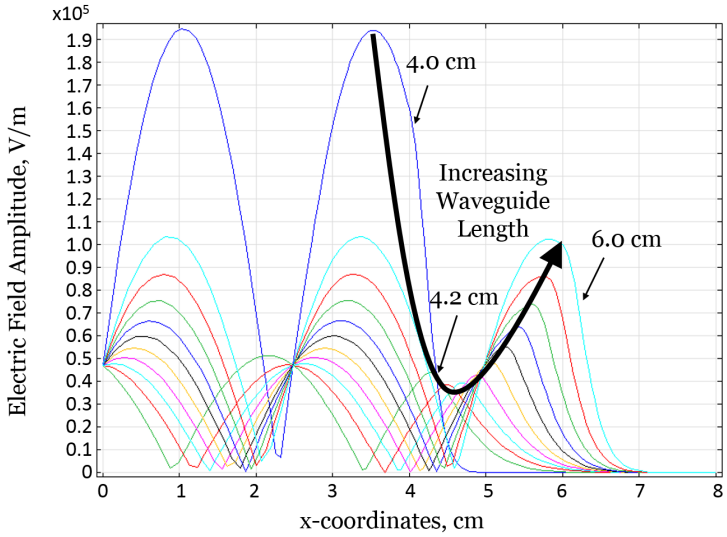

Figure 17. RF electric field amplitude curves for different waveguide lengths. At a critical waveguide length (4.0 cm in this case) for a fixed RF power (100 W), the electric field amplitude jumps in magnitude due to a cavity resonance condition. Note that the structure of the electric field amplitude repeats itself as the waveguide length continues to be increased.

density effectively acts as a conducting wall of a microwave cavity and is "tuning" the cavity as the critical plasma density moves. The effective microwave cavity length formed by the critical plasma density depth and the RF input boundary decreases as the plasma density shifts upstream with increasing RF power. Given a sufficient phase shift of the RF electric field due to this decreasing cavity length and the appropriate input waveguide length (or input RF electric field phase), the cavity abruptly becomes resonant as the reflected and incident RF waves interfere in a solely constructive manner as seen in both Figure 15 and Figure 16. This resonance causes the RF electric field amplitude to jump significantly.

The augmented RF electric field sharply increases the electron temperature in a small upstream region near the microwave window, causing an increase in the plasma density due to ionization, as well as an increase in the sheath voltage. The combination of increased particle thermal energies, sheath voltages, and number densities subsequently increases the plasma heating of the upstream portion of the emitter material. The upstream increase in emitter temperature, resulting in a maximum emission current upstream, causes a cascading effect in the downstream plasma density: the upstream emission current drives the local plasma density, which drives the downstream plasma heating of the emitter, and so forth throughout the entire emitter region.

The dependence of the jump on waveguide length (therefore on RF electric field phase) is shown in Figure 17. We note that the resonance repeats itself as the waveguide length continues to increase because of the repeating electric field phase and therefore a repeating resonance condition. Evidence of the repeating is shown in Figure 17, although, only one resonance is shown for simplicity.

After the jump transition, the upstream plasma density has reached a magnitude such that the incident RF wave is reflected at a minimum distance within the cathode, and further increases in RF power cause relatively small increases in peak plasma density, emission current, etc. We observe that further increasing the RF power does not transition the cathode operation away from the cavity resonance as the resonance is maintained for all of the post-critical RF powers considered.

V. Conclusion

The purpose of this paper was to explore the feasibility and behavior of a novel RF-Controlled Hollow Cathode concept in which RF power is added via waveguide to a bulk-emitting hollow cathode. The large

cathode diameter of the RF-CHC was determined by the RF waveguide geometry requirements. We modeled a microwave plasma inside a hollow cathode cavity using commercial finite element software, and we simplified the model by neglecting orifice effects and coupling to the external cathode plasma.

We found that adding RF power to a cathode cavity does affect the internal plasma in several ways. Increasing the RF power leads to higher plasma densities over most of the emitter length and shifts the maximum plasma density upstream along the cathode major axis. This behavior increases the extent of dense plasma contact with the emitter and broadens the plasma density profile. A large-diameter cathode, such as the RF-CHC, also improves expected operational lifetime by operating at lower emitter temperatures and increasing the upstream penetration of dense plasma contact. We expect that the RF-CHC will reach plasma densities on the order of 10^{18} to 10^{19} m^{-3} along the entire length of the emitter resulting in thermally-limited emission for nearly all of the emitter area.

Depending on the neutral gas flow rate, the RF power, and the incident RF electric field phase (or waveguide length), we found that a sharp "jump" occurs. This jump results in a substantial increase in the incident RF electric field magnitude, absorbed RF power, and plasma density. We found that the conditions under which the jump occurs depend on the gas pressure (therefore on flow rate and orifice size) and input RF power, where an increase in the latter can be used to reduce the required flow rate to reach the jump condition. We have shown that the jump behavior is due to a cavity resonance that occurs with the added RF waves. The critical plasma density at which incident RF waves are reflected is shifted with varying RF power, effectively creating a conducting cavity wall that moves axially to "tune" the RF electric field phase within the cavity. With the appropriate axial location of the critical plasma density, the incident and reflected RF waves constructively interfere to cause a jump in the RF electric field amplitude, creating a cascading effect on the plasma and the resulting emission throughout the cathode.

The overall performance of the RF-CHC is significantly improved after the observed jump when evaluated against our stated goals of decreasing peak current density for a given discharge current and increasing the maximum discharge current. We have verified the feasibility of the RF-CHC configuration from a first-order approach using numerical simulations and beneficial behaviors have been uncovered that merit further investigation in the form of higher fidelity simulations and experimentation.

Acknowledgments

This research has been supported by the U.S. Air Force Office of Scientific Research.

References

[1]Shastry, R., Herman, D. A., Soulas, G. C., and Patterson, M. J., "NASAs Evolutionary Xenon Thruster (NEXT) Long-Duration Test as of 736 kg of Propellant Throughput," 48th AIAA Joint Propulsion Conference, Atlanta, Georgia, 2012, pp. 1–20.

[2]Hofer, R. R., Randolph, T. M., Oh, D. Y., Snyder, J. S., and de Grys, K. H., "Evaluation of a 4.5 kW Commercial Hall Thruster System for NASA Science Missions," 42nd Joint Propulsion Conference, Sacramento, California, 2006.

[3]Capadona, L. A., Woytach, J. M., Kerslake, T. W., Manzella, D. H., Christie, R. J., Hickman, T. A., Scheidegger, R. J., Hoffman, D. J., and Klem, M. D., "Feasibility of Large High-Powered Solar Electric Propulsion Vehicles: Issues and Solutions," AIAA Space 2011 Conference, Long Beach, California, 2012.

[4]Brown, D. L., Beal, B. E., and Haas, J. M., "Air Force Research Laboratory High Power Electric Propulsion Technology Development," IEEEAC, 2009.

[5]Goebel, D. M., Jameson, K. K., and Hofer, R. R., "Hall Thruster Cathode Flow Impact on Coupling Voltage and Cathode Life," Journal of Propulsion and Power, Vol. 28, No. 2, March 2012, pp. 355–363.

[6]Soulas, G. C., Haag, T. W., Herman, D. A., Huang, W., Kamhawi, H., and Shastry, R., "Performance Test Results of the NASA-457M v2 Hall Thruster," 48th AIAA Joint Propulsion Conference, Atlanta, Georgia, 2012, pp. 1–17.

[7]Goebel, D. M. and Chu, E., "High Current Lanthanum Hexaboride Hollow Cathode 20-to-100 kW Class Hall Thrusters," 48th AIAA Joint Propulsion Conference, Atlanta, Georgia, 2012, pp. 1–11.

[8]Van Noord, J. L., Kamhawi, H., and Mcewen, H. K., "Characterization of a High Current, Long Life Hollow Cathode," 29th International Electric Propulsion Conference, Princeton, New Jersey, 2005, pp. 1–12.

[9]Katz, I., Mikellides, I. G., Goebel, D. M., and Polk, J. E., "Insert Heating and Ignition in Inert-Gas Hollow Cathodes," IEEE Transactions on Plasma Science, Vol. 36, No. 5, 2008, pp. 2199–2206.

[10]Goebel, D. M. and Katz, I., Fundamentals of Electric Propulsion: Ion and Hall Thrusters, Vol. 1, John Wiley & Sons Inc, 2008.

[11]Sarver-Verhey, T. R., "Scenario for Hollow Cathode End-of-Life," 26th International Electric Propulsion Conference, Kitakyushu, Japan, 1999, pp. 703–713.

[12]Goebel, D. M. and Chu, E., "High Current Lanthanum Hexaboride Hollow Cathodes for High Power Hall Thrusters," 32nd International Electric Propulsion Conference, Jet Propulsion Laboratory, Wiesbaden, Germany, 2011, pp. 1–16.

[13]Plasek, M. L., Jorns, B., Choueiri, E. Y., and Polk, J. E., "Exploration of RF-Controlled High Current Density Hollow Cathode Concepts," 48th AIAA Joint Propulsion Conference, Atlanta, Georgia, 2012, pp. 1–17.

[14]Foster, J. E. and Patterson, M. J., "Characterization of 40-Centimeter Microwave Electron Cyclotron Resonance Ion Source and Neutralizer," Journal of Propulsion and Power, Vol. 21, No. 5, 2005, pp. 1–5.

[15]Liao, S. Y., Microwave Devices and Circuits, 3rd ed., 1990.

[16]Lieberman, M. A. and Lichtenberg, A. J., Principles of plasma discharges and materials processing, John Wiley and Sons, April 1994.

[17]Jain, S. K., Jain, A., and Hannurkar, P. R., "Indigenous development of a low cost high power 2 kW (CW), 2 . 45 GHz microwave system," Indian Journal of Pure & Applied Physics, Vol. 42, 2004, pp. 896–901.

[18]Windes, D., Dutkowski, J., Kaiser, R., and Justice, R., "Triservice-NASA cathode life test facility," Applied Surface Science, Vol. 146, 1999, pp. 75–78.

[19]Dieumegard, D., Tonnerre, J. C., Brion, D., and Shroff, A. M., "Life Test Performance of Thermionic Cathodes," Applied Surface Science, Vol. 111, 1997, pp. 84–89.

[20]Salhi, A. and Turchi, P. J., "Scaling Relations for Design and Operation of Orificed-Hollow Cathodes," 30th Joint Propulsion Conference, Indianapolis, Indiana, 1994, pp. 0–7.

[21]Goebel, D. M., Watkins, R. M., and Jameson, K. K., "LaB6 Hollow Cathodes for Ion and Hall Thrusters," Journal of Propulsion and Power, Vol. 23, No. 3, May 2007, pp. 552–558.

[22]Goebel, D. M. and Watkins, R. M., "Compact Lanthanum Hexaboride Hollow Cathode," Review of Scientific Instruments, Vol. 81, No. 8, Aug. 2010, pp. 083504.

[23]Goebel, D. M., Jameson, K. K., Katz, I., and Mikellides, I. G., "Potential Fluctuations and Energetic Ion Production in Hollow Cathode Discharges," Physics of Plasmas, Vol. 14, No. 10, 2007, pp. 103508.

[24]Goebel, D. M., Jameson, K. K., Katz, I., and Mikellides, I. G., "Plasma Potential Behavior and Plume Mode Transitions in Hollow Cathode Discharges," 30th International Electric Propulsion Conference, Florence, Italy, 2007, pp. 1–9.

[25]Mikellides, I. G. and Katz, I., "Wear Mechanisms in Electron Sources for Ion Propulsion, 1: Neutralizer Hollow Cathode," Journal of Propulsion and Power, Vol. 24, No. 4, July 2008, pp. 855–865.

[26]Goebel, D. M., Mikellides, I. G., Polk, J. E., Young, J., Tighe, W. G., and Chien, K.-r., "Keeper Wear Mechanisms in the XIPS 25-cm Neutralizer Cathode Assembly," 31st International Electric Propulsion Conference, Ann Arbor, Michigan, 2009, pp. 1–11.

[27]Mikellides, I. G., Goebel, D. M., Snyder, J. S., Katz, I., and Herman, D. a., "The discharge plasma in ion engine neutralizers: Numerical simulations and comparisons with laboratory data," Journal of Applied Physics, Vol. 108, No. 11, 2010, pp. 113308.

[28]Chu, E., Goebel, D. M., and Wirz, R. E., "Reduction of Energetic Ion Production in Hollow Cathodes by External Gas Injection," Journal of Propulsion and Power, June 2013, pp. 1–9.

[29]Lafferty, J. M., "Boride Cathodes," Journal of Applied Physics, Vol. 22, No. 3, 1951, pp. 299.

[30]Polk, J. E., Capece, A. M., Mikellides, I. G., and Katz, I., "Barium Depletion in the NSTAR Discharge Cathode After 30,472 Hours of Operation," 46th Joint Propulsion Conference, Nashville, TN, 2010.

[31]Mikellides, I. G., Katz, I., Goebel, D. M., and Polk, J. E., "Hollow cathode theory and experiment. II. A two-dimensional theoretical model of the emitter region," Journal of Applied Physics, Vol. 98, No. 11, 2005, pp. 113303.

[32]Younglove, B. A. and Hanley, H. J. M., "Viscosity and Thermal Conductivity Coefficients of Gaseous and Liquid Argon," Journal of Physical Chemistry, Vol. 15, No. 4, 1986.

[33]Jones, T. J., Thermionic Emission, 1936.

[34]Hobbs and Wesson, "Heat flow through a Langmuir sheath in the presence of electron emission," Plasma Physics, Vol. 85, 1967.

[35]Schottky, W., "Concerning the Discharge of Electrons from Hot Wires with Delayed Potential," Annalen der Physik, Vol. 44, No. 15, 1914, pp. 1011– 1032.